Supporting Information

Switchable Circularly Polarized Luminescent Mn-Based Hybrid Metal Halides

Xuexia Yu,[a] Songbing Zhong,[a] Zeyi Guo,[a] Jia Guan,[a,b] Hao Tang,[a] Xiaolong He,[a,*] Yihuang Chen, [a,b,*] Shuang Pan[a,b,*]

[a] *Wenzhou Key Lab of Advanced Energy Storage and Conversion, Zhejiang Province Key Lab of Leather Engineering, College of Chemistry and Materials Engineering, Wenzhou University, Wenzhou, Zhejiang 325035, China*

[b] *Zhejiang Engineering Research Center for Electrochemical Energy Materials and Devices, Institute of New Materials and Industrial Technologies, Wenzhou University, Wenzhou, Zhejiang 325035, China*

Experimental sections

Chemicals

Manganese (II) acetate tetrahydrate ($MnAC_2.4H_2O$, 98%), ultra-dry N,N′-dimethylmethanamide (DMF, 99.8%) and HBr (48 wt% in water) were purchased from Shanghai Aladdin Biochemical Technology Co, Ltd**.** *S*-, *R*-, *rac*-2-methylpiperazine ($C_5H_{12}N_2$, 98%) were purchased from Shanghai Bide Pharmatech Co, Ltd. All the reagents were used without further purification.

Synthesis of bulk MPZMB single crystals

In a typical synthesis process, 2.54 g (10 mmol) of $MnAC_2 \cdot 4H_2O$ and 1 g (10 mmol) of 2-methylpiperazine (*R*-/*S*-/*rac*-MPZ) were added to a 20 mL glass bottle containing 10 mL of hydrobromic acid (48 wt% in water) and stirred at 60℃ until completely dissolved, resulting in a yellowish transparent single crystal precursor solution. Subsequently, the precursor liquid was transferred to a suitable-sized petri dish (the diameter of petri dish is 6 cm), sealed with plastic wrap with air holes. Following that, the solvent was allowed to evaporate slowly at 60° C until the crystals in the solution grew to a suitable size. Then, the solution was filtered while hot to collect the single crystals. The surface of the single crystals was washed multiple times with anhydrous ether to remove impurities, and they were dried under vacuum to obtain pure single-crystal samples. Additionally, before conducting single crystal diffraction tests, we cleaned the single crystals using epoxy adhesive to ensure their quality and purity.

Preparation of MPZMB polycrystalline film

MPZMB film was taken as an example. In the synthesis process of MPZMB for the preparation of polycrystalline film, 1 g of freshly synthesized single crystal was ground and added to a 20 mL glass bottle containing 5 mL of ultra-dry DMF (99.8%) solvent. The mixture was stirred at 50 °C until completely dissolved, resulting in a light yellow transparent single crystal solution (i.e., *R*-MPZMB ink). Subsequently, 100 μL of *R*-MPZMB ink was transferred onto a clean glass substrate (2 cm × 2 cm ×

1 mm), and then heated at 90°C for 20 mins to facilitate the film annealing process. Finally, a yellow transparent polycrystalline film exhibiting green fluorescence was obtained.

Preparation of MPZMB@PVP film

R-MPZMB@PVP film was taken as an example. During the preparation of MPZMB@PVP film, 1 g of freshly synthesized and ground single crystal powder is mixed with 4 g of PVP polymer. The mixture is added to a 20 mL glass bottle containing 5 mL of ultra-dry DMF (99.8%) solution and stirred at 50 °C until completely dissolved, resulting in a pale-yellow transparent solution (i.e., *R*-MPZMB@PVP ink). Subsequently, 100 μL of *R*-MPZMB@PVP ink was dropped onto a clean glass substrate (2 cm × 2 cm × 1 mm), and then heated at 90°C for 20 mins to facilitate the film annealing process. Finally, a transparent MPZMB@PVP film was obtained.

Stencil Printing

Stencil printing was performed utilizing a 10 cm × 6 cm hardwood screen printer with emulsion screens and polyester screen-printing mesh (100 mesh counts, threat per inch, for 150 μm openings, respectively). A polyurethane squeegee (≈45° angle with the mesh) was used to brush the ink on glass substrate with certain molds.

Material characterization

The single crystal X-ray diffraction (SC-XRD) test was conducted using a Smart APEXII (Bruker, Germany) single crystal diffractometer. Prior to loading the sample onto the machine, it is essential to select a high-quality crystal sample under the microscope. The SC-XRD analysis was performed at low temperature, and the resulting data was processed using Olex 2 software for structural analysis and crystal visualization. SEM images were captured using an FEI field emission electron microscope, specifically the Nano SEM 200 model. P-XRD measurements were

conducted utilizing a Bruker D8 Advance XRD system. Thermogravimetric analysis (TGA) was conducted in Diamond TG-DTA/Spectrum GX. After being dried at 90 ℃ for 24 h and then continuously evacuated to ensure the removal of surface moisture, the as-prepared single crystal powder was uniformly distributed in the crucible under a nitrogen atmosphere. The temperature range for the analysis was set between 40℃ and 600℃, with a heating rate of 10℃/min. Time-resolved photoluminescence (TRPL) spectra were recorded on an FLS 980 fluorimeter. X-ray Photoelectron Spectroscopy (XPS) was performed using the ESCALAB 250Xi model. The differential scanning calorimetry (DSC) tests were measured on the DSCQ1000 differential scanning analyzer. For each measurement, less than 10 mg of ground single crystal powder sample was evenly spread in the crucible, which was then sealed consistently. The photoluminescence spectrum was obtained using a Hitachi 5J1-0004 fluorescence spectrometer, with excitation provided by a 365 nm xenon lamp. UV-visible spectra, photoluminescence spectra, and circular dichroism (CD) spectra were measured using a Shimadzu UV-2600 spectrometer and an applied photophysical Chirascan CD spectrometer, respectively. The anisotropy factor[1, 2] (g_{abs}) was calculated as the following equation (1):

$$g_{abs}=\text{CD (mdeg)}/32980\times\text{Absorbance} \quad (1).$$

The circular polarization luminescence (CPL) emission spectrum was obtained using the CPL-300 instrument by JASCO. The chiral single crystal sample or polycrystalline film was placed in the sample tank of the instrument, with the excitation wavelength set at 365 nm. The scanning range was from 420 nm to 700 nm. The luminescent anisotropy factor[3, 4] (g_{lum}) was calculated as the following equation (2):

$$g_{lum} = \Delta I / I = 2\,(I_L - I_R) / (I_L + I_R) \quad (2)$$

I_L and I_R are the luminous intensity of LCP light and RCP light, respectively.

Preparation of green photoluminescence CP-LEDs based on MPZMB single crystal

As described in the preparation method previously reported[5, 6], green photoluminescence CP-LEDs were prepared by excitation of single crystal samples with 375 nm UV GaN chips. The *S*-/*R*-MPZMB single crystal sample was affixed onto the the GaN chip, sealed with a plastic protective cover, and assembled into an LED device for testing. The chiral MPZMB SCs was positioned on the GaN chip, applying a current of 300 mA and voltage of 3 V. Right-circularly polarized light and left-circularly polarized light are observed upon rotating the λ/4 wave plate to −45° and +45° relative to the polarization direction of the polarizer, respectively.[4]

Calculation details

Spin-polarized density functional theory (DFT) calculations were conducted using Vienna *Ab-initio* Simulation Package (VASP), utilizing the projector-augmented wave (PAW)[7, 8] potentials. The Perdew-Burke-Ernzerhof (PBE) functional[9], based on the generalized gradient approximation (GGA), was utilized to describe the electron-ion interactions and evaluate the exchange-correlation energies. A 1×4×1 Monkhorst-Pack grid of *k*-points was employed for geometric optimization without constraints, based on the experimentally characterized crystal structure. The convergence threshold was set at 10^{-5} eV for energy and 0.02 eV $Å^{-1}$ for force, utilizing 400 eV cutoff for the plane wave basis set. Band structure and density of states (DOS) calculations were performed to further investigate the electronic behaviors.

Table S1. Crystal data and structure refinement for *R*-/*S*-/*rac*-MPZMB.

Empirical formula	$C_{20}H_{56}Br_{16}Mn_4N_8$ (*R*-MPZMB)	$C_{20}H_{56}Br_{16}Mn_4N_8$ (*S*-MPZMB)	$C_5H_{14}Br_4MnN_2$ (*rac*-MPZMB)
Formula weight (g/mol)	1907.04	1907.04	476.76
Temperature (K)	153.0	183.00	183.00
Crystal system	monoclinic	monoclinic	monoclinic
Space group	$P2_1$	$P2_1$	$P2_1/n$
Unit cell dimensions (Å)	a=14.4751(19) b=9.1464(12) c=20.292(3) α=γ=90° β=97.663(4) °	a=14.5257(9) b=9.1150(6) c=20.4113(13) α=γ=90° β=97.657(2) °	a=8.7315(3) b=15.3631(5) c=10.1755(3) α=γ=90° β=90.4320(10)(4) °
Volume ($Å^3$)	2662.5(6)	2678.4(3)	1364.93(8)
Z	2	2	4
Density (g/cm^3)	2.379	2.365	2.320
F (000)	1784.0	1784.0	892.0
Independent reflections	7662 [R_{int} = 0.0334 , R_{sigma} = 0.0552]	8977 [R_{int} = 0.0460 , R_{sigma} = 0.0419]	2158 [R_{int} = 0.0322 , R_{sigma} = 0.0331]
Data/restraints/parameters	7662/1/438	8977/1/438	2158/0/110
Final R indexes [I>=2σ (I)]	R_1 = 0.0219, wR_2 = 0.0537	R_1 = 0.0286, wR_2 = 0.0722	R_1 = 0.0325, wR_2 = 0.0792
Final R indexes [all data]	R_1 = 0.0226, wR_2 = 0.0540	R_1 = 0.0289, wR_2 = 0.0724	R_1 = 0.0330, wR_2 = 0.0799
Largest diff. peak/hole ($e \cdot Å^{-3}$)	0.65/-0.58	1.71/-0.87	1.25/-0.96

Table S2. Summary of chiral manganese halides in recently published literature.

Chiral manganese halide	Dimensionality	Emission peaks (nm)	PLQYs (%)	g_{lum}-Factor	*Ref.*
R-, *S and rac*-(2-methylpiperazine) $MnBr_3$	0D	530	12	1.12×10^{-2}	This work
(*R*)- and (*S*)-3-(fluoropyrrolidinium)$MnBr_3$	1D	550–750	32.46	$\pm 6.1 \times 10^{-3}$	*J. Am. Chem. Soc*. 2020, 142, 4756−4761
(*R*/*S*-1-PPA)$_2MnBr_4$	0D	510	13	-10^{-2} (R)	*Journal of Alloys and Compounds,* 2022, 910, 164892
(*R*/*S*-3-quinuclidinol)$MnBr_3$	1D	620	50.2	3.27×10^{-1} for single crystal, 2.3×10^{-2} for	*Angew. Chem. Int. Ed*. 2022, 61, e202205906

				polycrystalline	
(*R/S*-3-quinuclidinol)$_2$MnBr$_4$	0D	520	22.6	8.2×10^{-3} for polycrystalline	
(D)- and (L)-(tert-butyl prolinate)MnCl$_3$	1D	646	67	6.3*10^{-3}	*Chem. Eur. J.* 2022, 28, e202201
(*R*/*S*-MBA)MnCl$_3$·CH$_3$OH (MBA =C$_6$H$_5$CH(CH$_3$)NH$_3^+$)	1D	660	-	1.25 × 10^{-2}	*Adv. Optical Mater*. 2023, 2301272
R/*S*-[MBA-Me$_3$]MnBr$_4$	0D	520–550	98	4.5 × 10^{-3}	*Adv. Optical Mater*. 2023, 2202811
(*R*-/*S*-Br MBA)$_3$MnBr$_5$	0D	634	-	3.6×10^{-4} (R)	*J. Mater. Chem. C,*

				and 4.2×10^{-4} (S)	*2023,11, 5461-5468*
(*R*/*S*-3-aminopyrrolidine dihydrochloride)$_6$(Mn_3Cl_{12})$(Cl)_6$	1D	638	42	7.1×10^{-3}	*J. Mater. Chem. C, 2023,11, 3206-3212*
(*R*/*S*-1,2-diaminopropane dihydro chloride)$_3$(Mn_3Cl_{12})		650	85	7.1×10^{-3}	

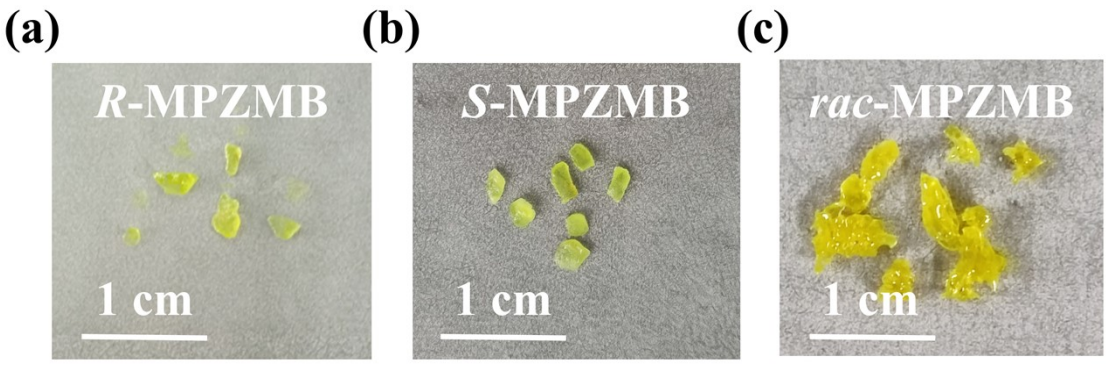

Figure S1. The digital photographs of obtained single crystal samples: (a) *R*-MPZMB (b) *S*-MPZMB and (c) *rac*-MPZMB.

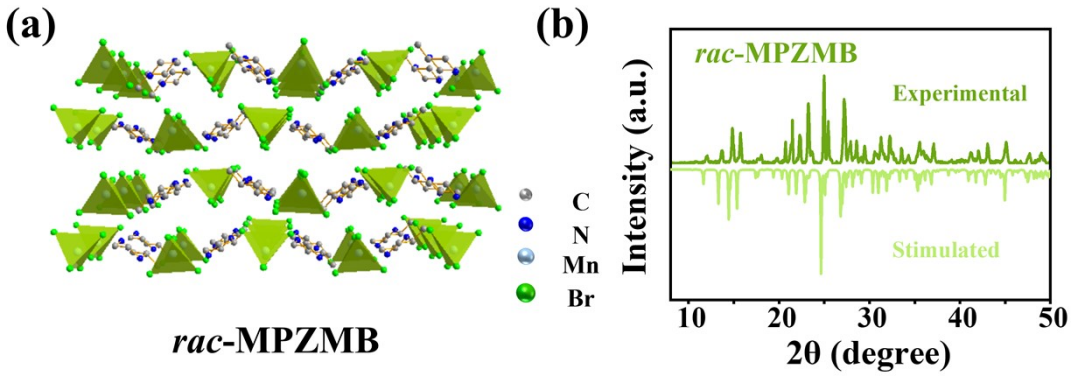

Figure S2. (a) Single crystal structure, and (b) PXRD pattern and the corresponding simulated peaks from SCXRD of *rac*-MPZMB.

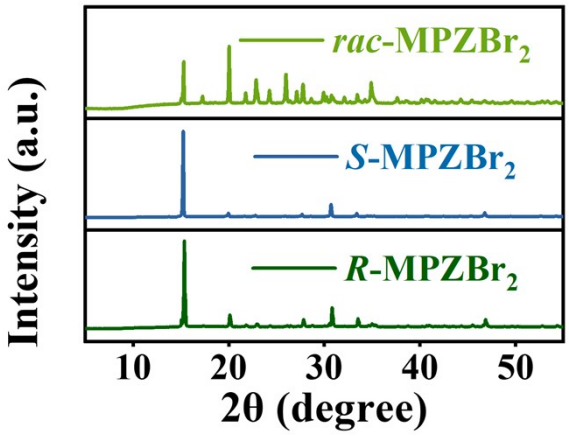

Figure S3. PXRD patterns of *R*-$MPZBr_2$, *S*-$MPZBr_2$ and *rac*-$MPZBr_2$.

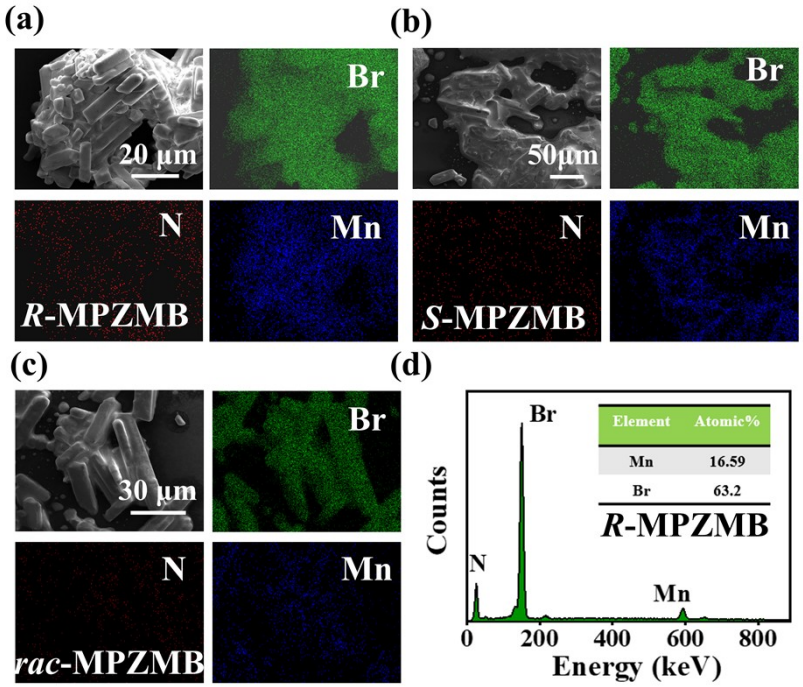

Figure S4. EDS elemental mappings of (a) *R*-MPZMB (b) *S*-MPZMB and (c) *rac*-MPZMB, and (d) the Energy dispersive spectrum of *R*-MPZMB. The inset table provides the percentage of the corresponding element content of the prepared *R*-MPZMB sample.

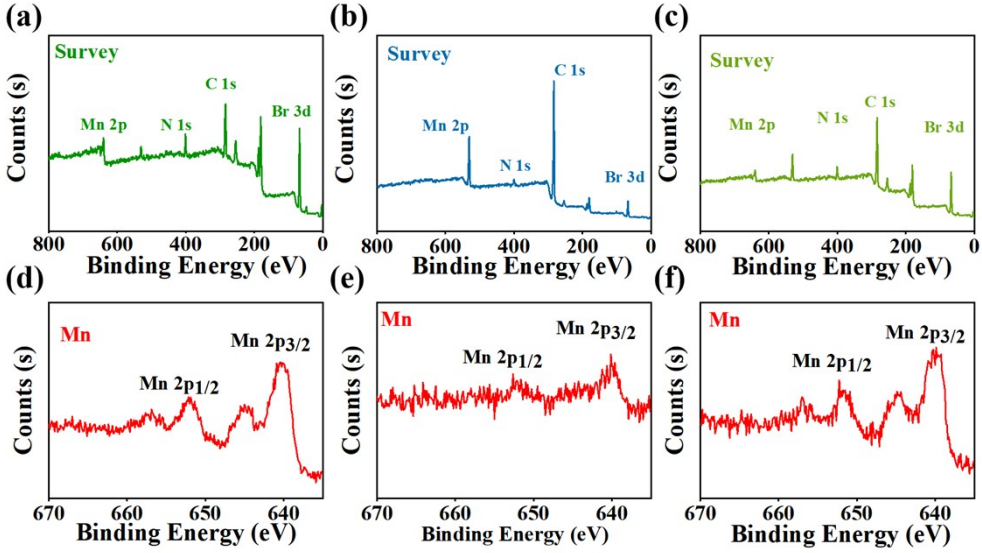

Figure S5. (a-c) X-ray photoelectron spectroscopic (XPS) analysis and (d-e) the high-resolution spectra of Mn 2p of *R*-/*S*-/*rac*-MPZMB, respectively.

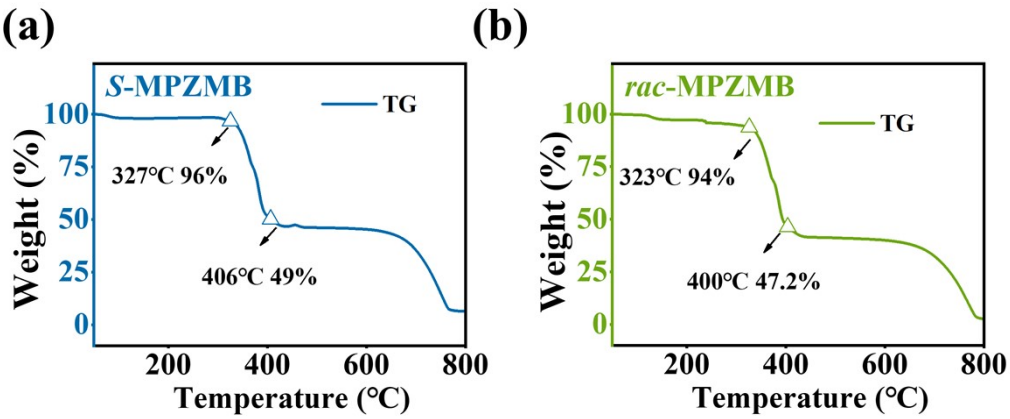

Figure S6. The TGA results of (a) *S*-MPZMB and (b) *rac*-MPZMB.

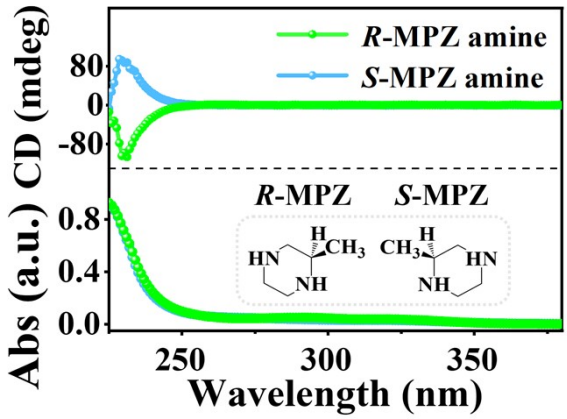

Figure S7. CD and corresponding absorption spectra of *R*-, *S*-MPZ amines. The illustration shows the molecular structure of *R*-MPZ and *S*-MPZ amine.

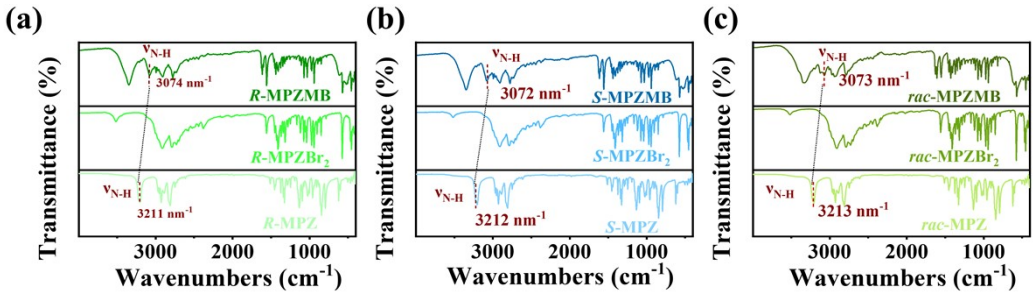

Figure S8. The FTIR spectra of (a) *R*-MPZMB, (b) *S*-MPZMB, (c) *rac*-MPZMB, along with the corresponding precursor amine and its halide salts. The red dotted line represents N-H stretching vibration $\nu_{N\text{-}H}$.

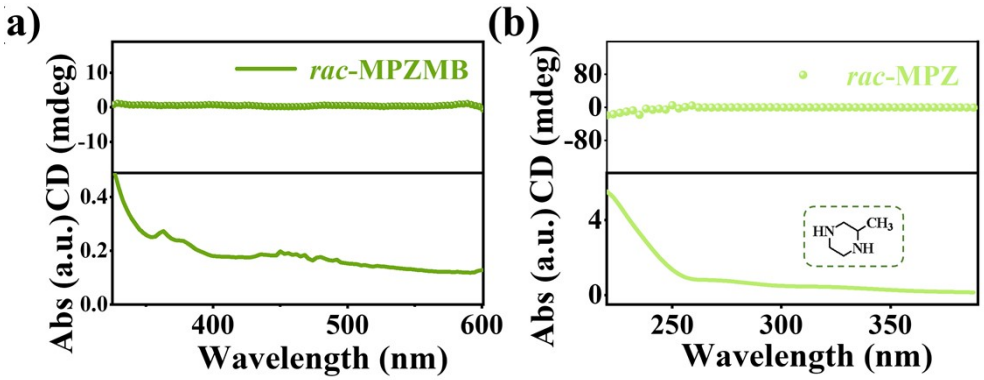

Figure S9. CD spectra and absorption spectra of (a) *rac*-MPZMB film and (b) the corresponding organic amine. The inset is the scheme of molecular structure of *rac*-2-methylpiperazine.

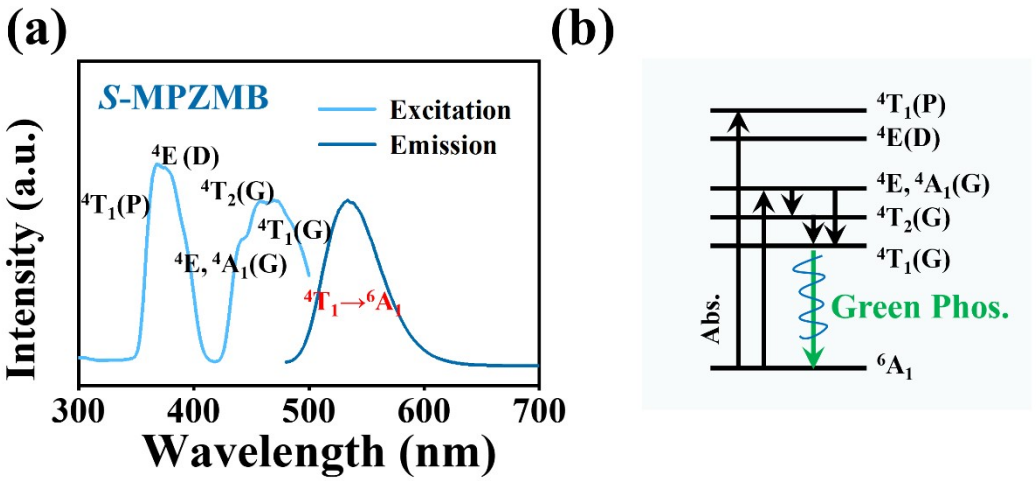

Figure S10. Photoluminescence excitation and emission spectra of (a) *S*-MPZMB and (b) schematic diagram of the luminescence process of *S*-MPZMB.

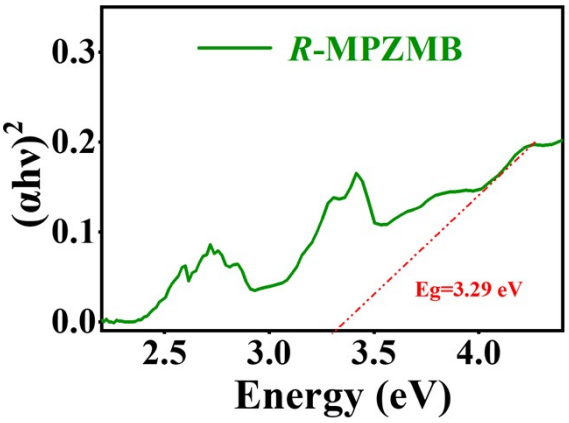

Figure S11. The corresponding tauc plots of *R*-MPZMB.

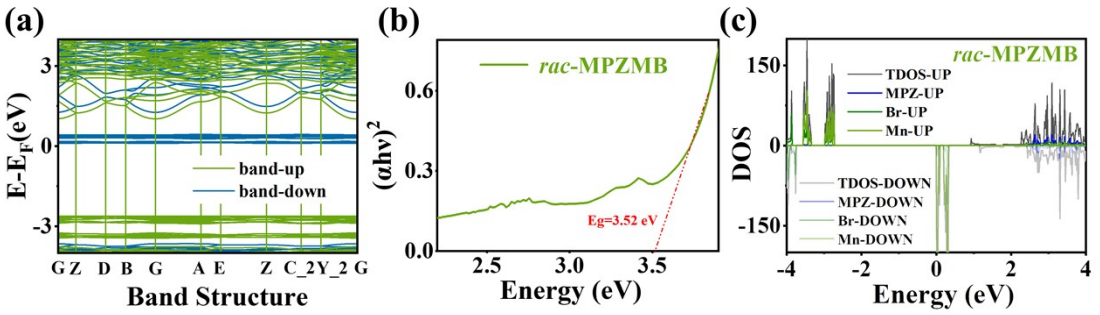

Figure S12. (a) The electronic band structure, (b) tauc plots and (c) total and orbital-projected PDOSof *rac*-MPZMB.

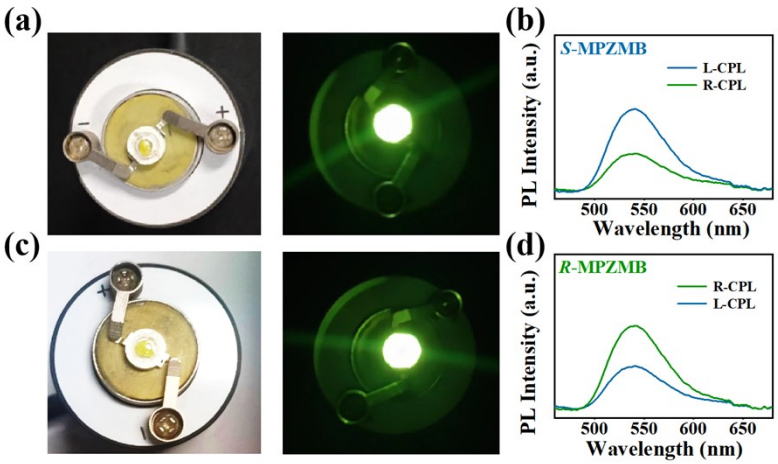

Figure S13. Digital photos of (a) *S*-MPZMB-based CP-LED and (c) *R*-MPZMB-based CP-LED. (b) L-CPL and (d) R-CPL light selectivity of MPZMB-based CP-LED. I_L and I_R mean the intensity of L- and R-CPL, respectively.

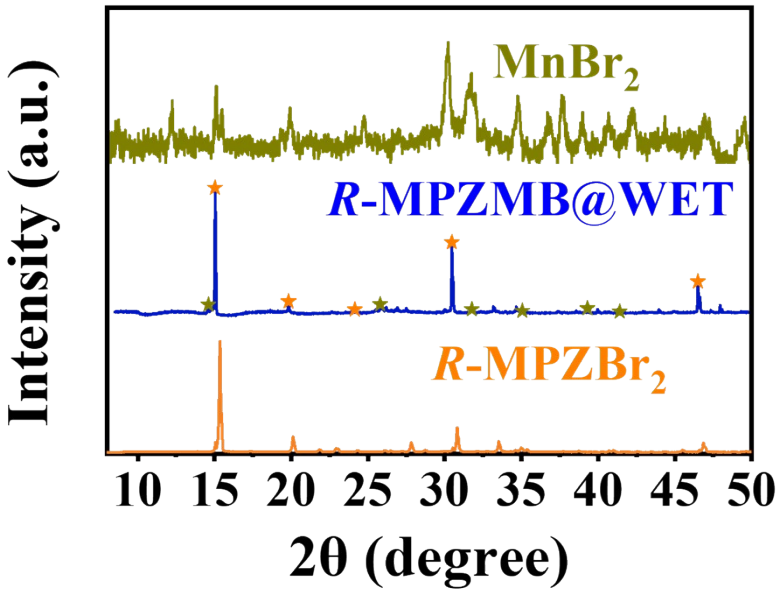

Figure S14. PXRD pattern of *R*-MPZMB@WET powder, along with comparative results with the precursor materials.

Figure S15. Digital images captured under UV light, depicting the continuous fluorescence change process. (a) The fluorescence change of R-MPZMB@WET powder during the heating process, wherein the sample was heated to 100 ℃ and then to 150 ℃ before cooling to room temperature. (b) The fluorescence change during the cooling process in the nitrogen glove box, which is maintained at low oxygen and humidity conditions. (c) The sample being removed from the glove box and exposed to air with 70±50% relative humidity.

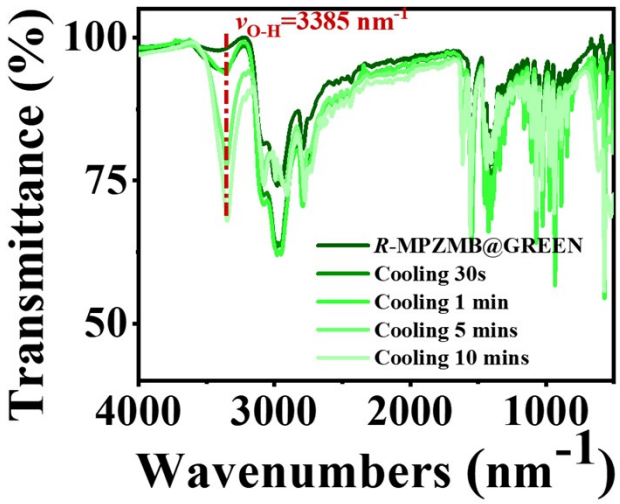

Figure S16. The time-dependent FTIR spectra of *R*-MPZMB@GREEN during cooling in the air.

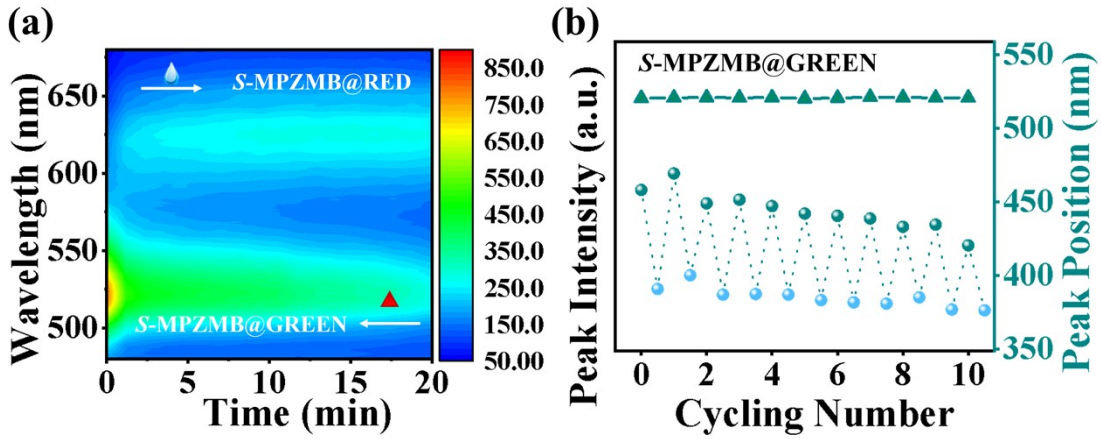

Figure S17. (a) Pseudocolor map of PL spectra from *S*-MPZMB@GREEN to *S*-MPZMB@RED going through a cooling process in the air (70 ± 5 % RH) at RT. (b) The corresponding change in PL intensity and peak position for *S*-MPZMB@GREEN over successive 10 cooling-heating cycles.

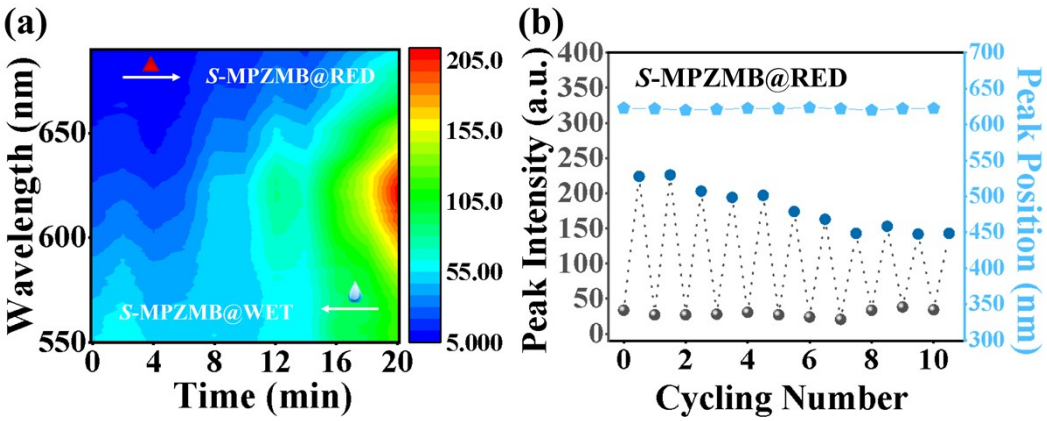

Figure S18. (a) Pseudocolor map of PL spectra from *S*-MPZMB@WET to *S*-MPZMB@RED going through a heating process at 100 °C for 20 min. (b) The change of PL intensity and peak position of *S*-MPZMB@WET over successive 10 heating-cooling cycles.

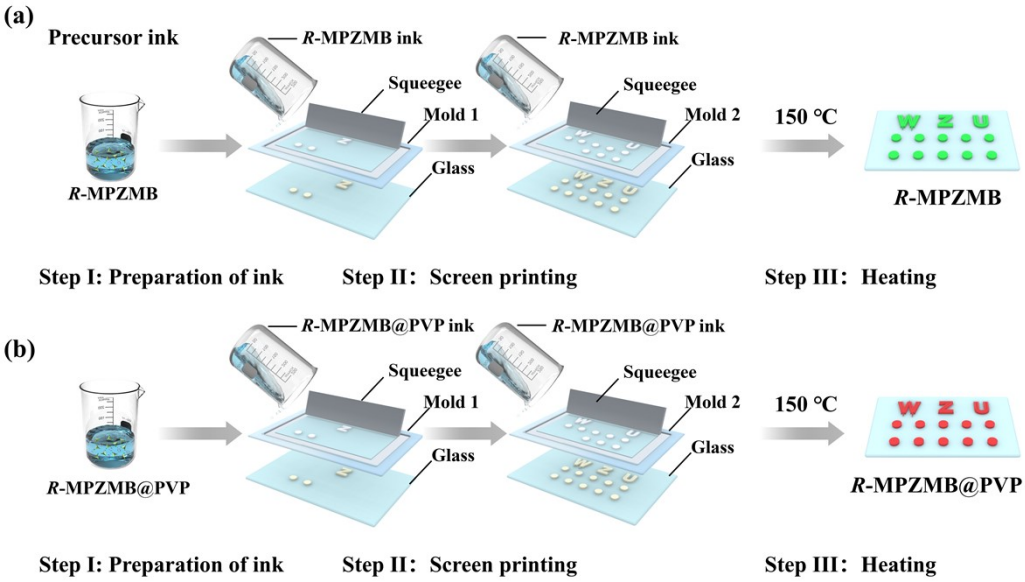

Figure S19 Schematic diagram of the screen printing of anti-counterfeiting patterns made with (a) *R*-MPZMB and (b) *R*-MPZMB@PVP inks，respectively.

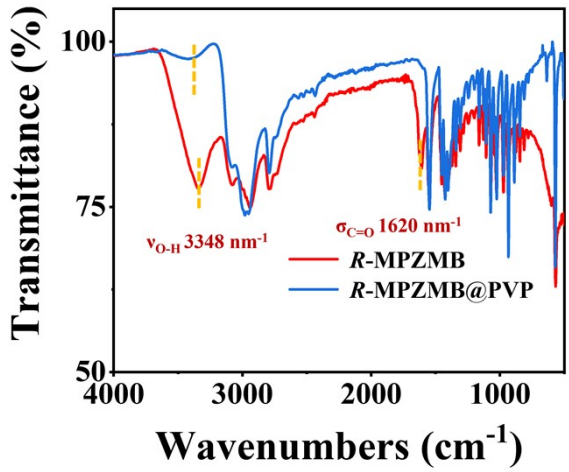

Figure S20. The FTIR spectra of *R*-MPZMB@PVP and *R*-MPZMB.

Reference

1. A. Ishii and T. Miyasaka, *Science Advances*, 2020, **6**, eabd3274.
2. R. Lu, Z. Wen, M. Zhao, J. Li, L. Zhang, Y. Yang, H. Jin, Y. Chen, S. Wang and S. Pan, *Advanced Optical Materials*, 2023, **11**, 2202290.
3. S. Ma, J. Ahn and J. Moon, *Advanced Materials*, 2021, **33**.
4. P. Zhang, R. Lu, Y. Chen, H. Wang, M. Zhao, L. Zhang, H. Jin, S. Wang, Y. Chen and S. Pan, *Chemical Engineering Journal*, 2024, **480**, 148306.
5. Z. Wen, R. Lu, F. Gu, K. Zheng, L. Zhang, H. Jin, Y. Chen, S. Wang and S. Pan, *Advanced Functional Materials*, 2023, **33**, 2212095.
6. R. Lu, Z. Wen, P. Zhang, Y. Chen, H. Wang, H. Jin, L. Zhang, Y. Chen, S. Wang and S. Pan, *Small*, **n/a**, 2311013.
7. P. E. Blochl, *Phys Rev B Condens Matter*, 1994, **50**, 17953-17979.
8. G. Kresse and D. Joubert, *Physical Review B*, 1999, **59**, 1758-1775.
9. John, P., Perdew, Kieron, Burke, Matthias and Ernzerhof, *Physical Review Letters*, 1997.